J Adv Ceram

Research Article

$BaTiO_3$-based multilayer ceramic capacitors with superior stability in energy-storage and pulse properties

Peiyao Zhao[1], Ying Jiang[1], Hongxian Wang[2], Limin Guo[3,✉], Xiaohui Wang[1,✉]

Cite this article: Zhao P, Jiang Y, Wang H, et al. *J Adv Ceram* 2026, **15**(4): 9221264. https://doi.org/10.26599/JAC.2026.9221264

ABSTRACT: Dielectric capacitors exhibiting high energy-storage properties and excellent pulse performance are critical components in advanced pulsed power systems. Multilayer ceramic capacitors (MLCCs) are the most widely used capacitors due to their high integration and excellent high-temperature endurance. Nevertheless, achieving high energy density and reliable performance over a wide temperature range and prolonged cycling remains the major challenge for existing commercial MLCCs based on linear dielectrics or Pb-based antiferroelectrics. Herein, we developed $BaTiO_3$-based relaxor ferroelectric MLCCs with X9S characteristics for high-voltage applications. The $BaTiO_3$-based MLCCs exhibit a good energy density of 6.09 J cm^{-3} and an ultrahigh efficiency of 98.2%, with superior stability in temperature (< 10%, 24–250 °C) and fatigue (after 10^6 cycles, < 4% at 200 °C). The pulse properties of MLCCs show minimal variation (< 4.5%, 22–200 °C). Moreover, 6878-size MLCCs with 300 nF can release a peak current of 3600 A at a rated voltage of 3000 V, which exhibits higher peak currents than linear MLCCs and better stability than Pb-based MLCCs. The excellent performance and superior stability demonstrate that relaxor ferroelectric MLCCs have great potential for advanced energy storage and pulsed power applications.

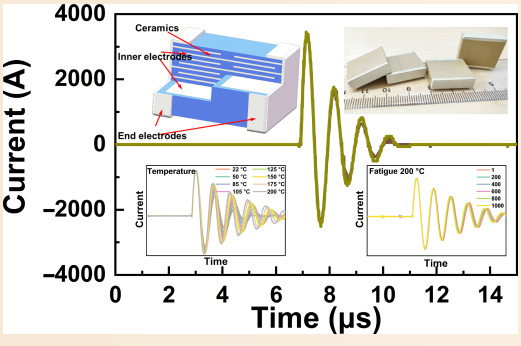

KEYWORDS: superior stability; multilayer ceramic capacitor (MLCC); energy storage; pulsed power; $BaTiO_3$-based relaxor ferroelectric

1 Introduction

Dielectric capacitors with ultrahigh power density are fundamental passive electronic components that can release stored energy within microseconds [1–4]. Their superior pulse properties make them widely used in advanced pulsed power systems [5–7]. The rapid advancement of third-generation semiconductor technology and hybrid electric vehicles has further stimulated extensive research into dielectric capacitors with enhanced energy storage and power pulse properties [8].

Multilayer ceramic capacitors (MLCCs), with multilayered structures of alternating ceramic and electrode layers, exhibit excellent high-temperature endurance, compact sizes, and high capacitance density [9]. The low equivalent series resistance and inductance of MLCCs can contribute to the excellent pulse properties. The properties of MLCCs are governed by both dielectric ceramics and structure design. A higher applied electric field enables a higher energy density (W_d, as shown in Fig. S1 in the Electronic Supplementary Material (ESM)) and power density (P_D) [10]. The reduction in ceramic layer thickness enables an exponential enhancement in breakdown strength (E_b) [11]. Commercial MLCCs for energy storage and pulsed power applications are primarily based on linear dielectric ceramics and Pb-based antiferroelectric (AFE) ceramics. However, linear MLCCs exhibit low W_d, primarily due to the low dielectric constant and maximum polarization (P_{max}). AFE MLCCs are limited by poor energy efficiency (η), reliability and temperature stability resulting from the AFE-FE phase transition [2,12]. These shortcomings have become the major bottleneck restricting the performance enhancement and application development of current commercial MLCCs.

The relaxor ferroelectric (RFE) with coexisting multiphase polar nanoregions holds promise for simultaneously achieving high W_d and good stability, attracting significant research interest [7,13–18]. The currently reported RFE MLCCs generally possess a dielectric layer thickness of < 20 μm and breakdown voltage of < 2000 V [7,15,19–22]. Their performance is difficult to compare against commercial MLCCs with high rated voltage (V_r) > 2000 V, as V_r is generally set at 30%–80% of the breakdown voltage. Herein, we fabricated MLCCs with a similar structural design to

[1] State Key Laboratory of New Ceramic Materials, School of Materials Science and Engineering, Tsinghua University, Beijing 100084, China. [2] Beijing Yuanliu Hongyuan Electronic Technology Co., Ltd., Beijing 100070, China. [3] State Key Laboratory of Information Photonics and Optical Communications, School of Physical Science and Technology, Beijing University of Posts and Telecommunications, Beijing 100876, China.

✉ Corresponding authors. E-mail: L. Guo, guolimin@bupt.edu.cn; X. Wang, wxh@mail.tsinghua.edu.cn

Received: November 24, 2025; Revised: February 11, 2026; Accepted: February 13, 2026

commercial high-voltage MLCCs, employing $BaTiO_3$-based (BT-based) RFE as the dielectric material. The BT-based RFE material is a weakly coupled BT-BiMO_3 RFE material that has been thoroughly investigated in our prior study [23]. The BT-based RFE MLCCs with V_r of 3000 V demonstrate an ultrahigh η of 98.2% at room temperature, with superior stability in temperature (< 10%, 24–250 °C) and fatigue (after 10^6 cycles, < 0.5% at 23 °C, < 4% at 200 °C) for energy-storage properties. The pulsed discharge properties remain virtually unchanged over the temperature range of 22–200 °C. Furthermore, 6878-size MLCCs with a capacitance of 300 nF were fabricated, which exhibit a higher discharge current than linear MLCCs and better temperature stability than Pb-based AFE MLCCs. Therefore, RFE MLCCs possess considerable potential for high-voltage applications in advanced energy storage and pulsed power devices and show significant promise for expanding the range of available material systems.

2 Experimental

2.1 MLCC preparation

The BT-based RFE material has a composition of $0.87BaTiO_3$–$0.13Bi(Zn_{2/3}(Nb_{0.85}Ta_{0.15})_{1/3})O_3$ and exhibits a pseudocubic perovskite structure (Fig. S2 in the ESM). The powders were synthesized by the traditional solid-state method [23], with high-purity oxides and carbonates (≥ 99.5%) as the raw materials. The weighted stoichiometric raw materials were mixed by ball-milling in water for 4 h. After drying, the mixtures were calcined at 900 °C for 5 h. The particle size distribution is shown in Fig. S3 in the ESM. Using a mixed solution of toluene and ethanol as the solvent, the calcined ceramic powders were ball-milled with an appropriate amount of solvent and dispersant for 6 h. Polyvinyl butyral was predissolved in the above solvent to serve as the binder. Then, the binder and dioctyl phthalate (as a plasticizer) were added to the well-dispersed slurry. The dispersant, binder, and plasticizer are added at concentrations of 2, 8, and 2 wt% relative to the ceramic powder, respectively. After ball milling for 18 h, a homogeneous slurry with appropriate viscosity was obtained. After tape-casting, uniform green tapes were obtained. The green tapes screen-printed with 70Ag-30Pd pastes as the inner electrode were stacked layer by layer with 10 (for 1210-MLCCs) and 100 (for 6878-MLCCs) active dielectric layers. The stacked samples were diced into standard 1210- and 6878-size MLCCs according to the inner electrode pattern. The MLCC green bodies were first burned at 600 °C for 5 h to remove the organics and then sintered at 1150 °C for 3 h with a heating rate of 5 °C min^{-1}. After natural cooling to room temperature, dense MLCC samples were obtained. Finally, the silver pastes were used as the end electrodes for electrical measurement. The sizes of 1210-MLCCs (10 active layers) and 6878-MLCCs (100 active layers) are 3.13 mm × 2.45 mm × 1.50 mm and 19.51 mm × 17.11 mm × 5.08 mm, respectively. The V_r of the MLCCs is designed as 3000 V.

2.2 Microstructure and electrical measurements

The crystal structure of dielectric ceramics was characterized by XRD with Cu Kα radiation (D8 Advance, Bruker, Germany). The microstructure of the MLCCs was observed by using SEM (Merlin VP compact, Zeiss, Germany) and an optical microscope (Olympus, Japan). Temperature-dependent capacitance and loss were characterized by an LCR meter (E4980A, Keysight, USA). The hysteresis loops of the MLCCs were characterized by a ferroelectric measurement system (TF Analyzer 2000E, aixACCT, Germany). The pulsed charge–discharge properties were characterized by a test system (CFD-003, TG Technology, China).

The calculation formula of the temperature coefficient of capacitance, Weibull distribution analysis, energy-storage properties, and pulsed charge–discharge properties are provided in the ESM.

3 Results and discussion

3.1 Microstructure

Figure 1(a) shows the structure of the MLCC, illustrating the arrangement of the inner electrodes and dielectric layers. MLCCs are designed with floating inner electrodes to achieve a higher

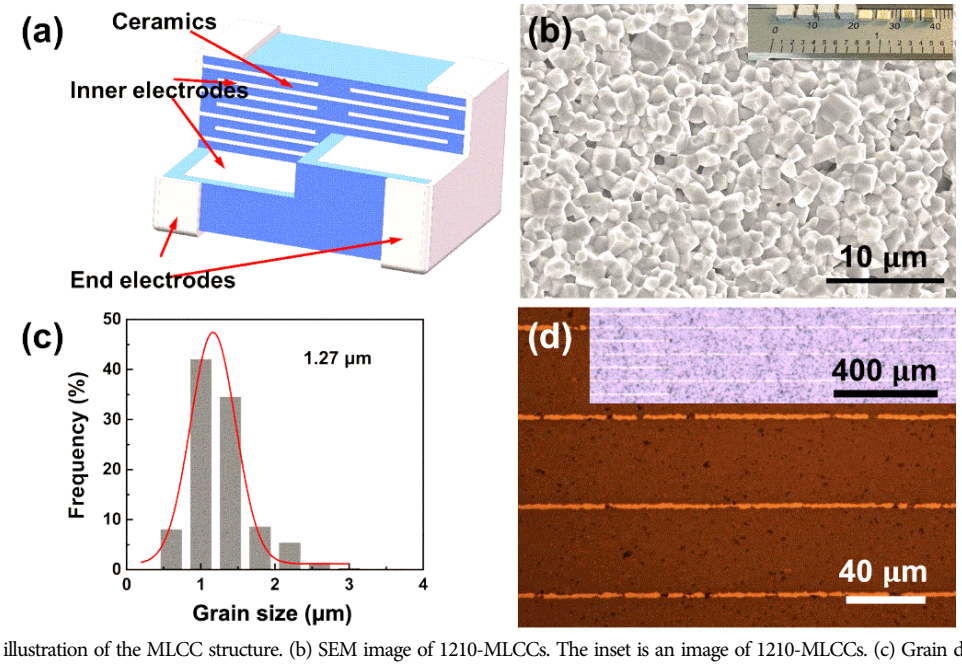

Fig. 1 (a) Schematic illustration of the MLCC structure. (b) SEM image of 1210-MLCCs. The inset is an image of 1210-MLCCs. (c) Grain distribution. (d) Optical microscopy images of the cross-section of MLCCs. The inset shows the floating inner electrode.

breakdown voltage via the series connection of capacitors. The sintered MLCCs demonstrate a dense microstructure with no detectable porosity and have an average grain size of approximately 1.27 μm, as shown in Figs. 1(b) and 1(c). Figure 1(d) and Fig. S4 in the ESM present the cross-section images of the MLCCs. It can be observed that the MLCCs possess dense microstructures and continuous inner electrodes. The continuous electrodes can contribute to a high breakdown electric field and excellent fatigue reliability. The thicknesses of the dielectric layers and electrodes are 43 and 2 μm, respectively. Hence, the rated electric field corresponding to V_r is approximately 34.9 V μm^{-1}.

3.2 Energy storage properties

The temperature-dependent capacitance and loss of 1210-MLCCs are shown in Fig. 2(a) and Fig. S5 in the ESM. The MLCCs exhibit an excellent temperature stability of capacitance, with a variation of ≤ ±22% relative to the value at room temperature over the temperature range of −55 to 200 °C, meeting the EIA X8R and X9S specifications. The dielectric constant peaks shift toward higher temperatures with increasing frequency, exhibiting a typical relaxor-like characteristic. The stable capacitance and dielectric constant originate from the multiphase coexistence and diffuse phase transition in relaxor ferroelectrics. This leads to a minimal temperature dependence of polarization, thereby ensuring remarkable temperature stability in both energy storage and pulse properties [12]. Moreover, low dielectric loss (< 1%) is achieved over a wide temperature range from 25 to 250 °C, which contributes to high η. The Weibull distribution analysis was employed to evaluate the E_b of 1210-MLCCs in Fig. 2(b) [24]. The E_b value is 86.3 V μm^{-1}, which is approximately 2.5 times the rated electric field. The Weibull modulus (m) value is 10.4, indicating a homogenous and reliable E_b data distribution. The unipolar P–E loops of 1210-MLCCs measured at room temperature and various electric fields are shown in Fig. 2(c). The hysteresis and P_r (remnant polarization) of the P–E loops exhibit negligible improvement with increasing applied electric field (Fig. S8(a) in the ESM), leading to a stable η. The maximum applied electric field of 1210-MLCCs at room temperature reaches 67.4 V·μm^{-1}, with a P_{max} of 27.8 μC·cm^{-2} and a remarkable P_r of 0.1 μC·cm^{-2}. Consequently, excellent energy-storage properties were achieved, with a W_d of 6.09 J·cm^{-3} and an ultrahigh η of 98.2%. The ultrahigh η can prevent thermal generation during operation, thereby enhancing the reliability [25].

3.3 Superior stability in energy-storage properties

During operation, the capacitors may undergo significant temperature fluctuations. Hence, the temperature stability of energy-storage properties is essential [5]. The unipolar P–E loops of 1210-MLCCs under V_r measured over a temperature range of 24–250 °C are displayed in Fig. 3(a). The P_{max} gradually decreases with increasing temperature, which is consistent with the trend observed in the dielectric properties [26]. Meanwhile, P_r remains unchanged along with the maintained slim P–E loops across the temperature range, ensuring ultrahigh η. With T_m (the temperature corresponding to the peak of the dielectric constant) below room temperature, the increasing paraelectric phase fraction at high temperature optimizes the dielectric nonlinearity, leading to more linear P–E loops [27–30]. Owing to the synergistic effect of these factors, the 1210-MLCCs achieve outstanding temperature stability in the energy-storage properties, as shown in Fig. 3(c). The W_d exhibits remarkable stability, within a minimal variation of < 10% between 24 and 250 °C. The η

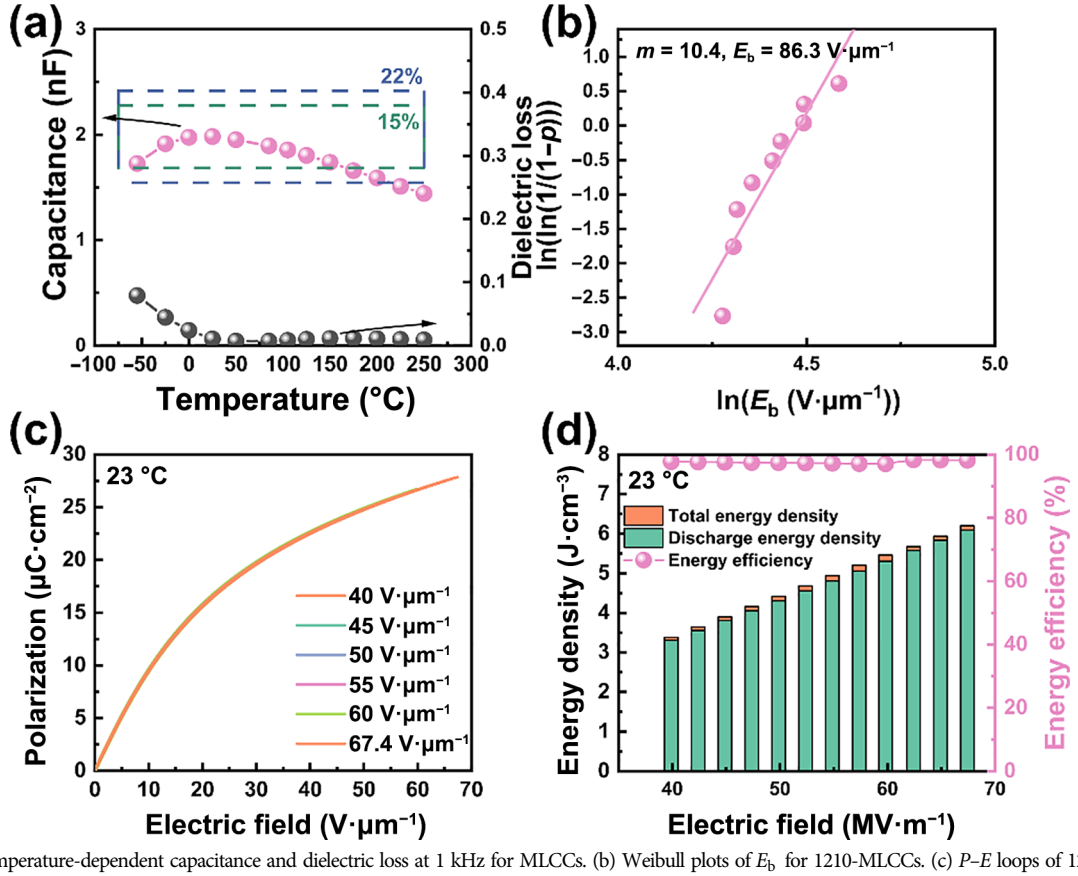

Fig. 2 (a) Temperature-dependent capacitance and dielectric loss at 1 kHz for MLCCs. (b) Weibull plots of E_b for 1210-MLCCs. (c) P–E loops of 1210-MLCCs at various electric fields and room temperature. (d) Corresponding energy-storage properties at room temperature.

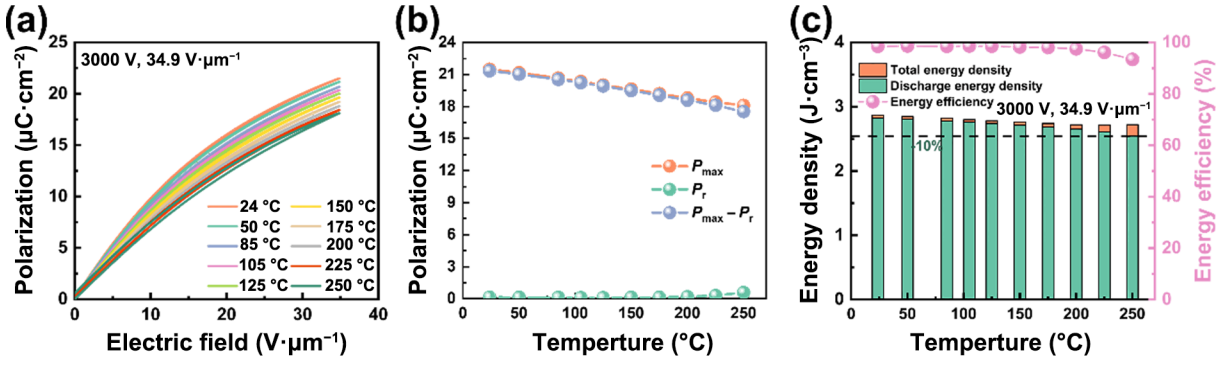

Fig. 3 (a) Temperature-dependent unipolar P–E loops of 1210-MLCCs under V_r. (b) P_{max}, P_r, and $P_{max}-P_r$ values of MLCCs under V_r as a function of temperature. (c) Temperature-dependent energy-storage properties of 1210-MLCCs under V_r.

decays merely 5% and remains > 93% even at 250 °C. The outstanding temperature stability of MLCCs underscores the significant potential for advanced energy-storage applications under varying thermal conditions.

The reliability of capacitors is another critical consideration for practical applications. The fatigue stability of 1210-MLCCs under different conditions was evaluated, as summarized in Fig. 4. After 10^6 cycles at room temperature and V_r, the P–E loops of 1210-MLCCs exhibit negligible degradation (Fig. S8(b) in the ESM), with variations of < 0.5% for W_d and η. Even when the temperature is raised to 200 °C, noticeable deterioration in the P–E loops and energy-storage properties occurs after more than 10^5 cycles (Fig. S8(c) in the ESM), with the changes remaining < 4%. The stable W_d and ultrahigh η of > 95% demonstrate the excellent fatigue stability of 1210-MLCCs. To further evaluate the reliability of 1210-MLCCs, the P–E loops and energy-storage properties at the maximum applicable electric field were compared under varying measurement conditions for three randomly selected samples. The corresponding results are presented in Figs. 4(e) and 4(f), Fig. S8(d) in the ESM, and Table 1. The W_t is the total energy density. Samples 1 and 2 were labeled according to their test temperatures of 23 °C and 200 °C, respectively. Sample 3 (labeled 200 °C-fatigue) was cycled 10^6 times under V_r at room temperature as well as 200 °C and then tested at 200 °C. Compared to Samples 1, 2, and 3 show a slight reduction in P_{max}, owing to the decrease in the dielectric constant at elevated temperature. Furthermore, the activation of defects in dielectric ceramics at 200 °C contributes to a rising P_r and loss, consequently leading to a deterioration in η and E_b. Despite undergoing 10^6 cycles at both room temperature and 200 °C, the energy-storage properties of MLCCs at 200 °C show no evident change compared to the uncycled sample. Moreover, the energy-storage properties of Sample 3 degrade by < 5% relative to the pristine sample, demonstrating the excellent fatigue stability and reliability of MLCCs.

3.4 Superior pulse properties

In many pulsed-power applications, the pulse properties of capacitors receive greater attention compared to the energy-storage properties. The overdamped and undamped pulsed discharge current curves of 1210-MLCCs at room temperature and various voltages are presented in Fig. S9 in the ESM. The peak values (I_{max}) of the overdamped and undamped discharge currents increase with the applied voltage, leading to increasing W_d and P_D. Due to the dielectric nonlinearity of relaxor ferroelectrics, the discharge time ($t_{0.9}$, the time taken to release 90% oftotal discharge energy) gradually decreases as the applied voltage increases. The temperature-dependent pulsed discharge properties under overdamped and undamped conditions at V_r are shown in Fig. 5. The overdamped and undamped discharge currents exhibit negligible changes across the temperature range from 22 to 200 °C. The I_{max} values of the overdamped and undamped discharge currents were observed to vary between 22.7–24.4 and 86.9–90.7 A, respectively. The discharge energy, calculated from the overdamped discharge current curves at various temperatures, is shown in Fig. 5(b). The values range from 3.1 to 3.2 mJ, exhibiting a decay of < 0.3% at 200 °C compared to room temperature. This superior temperature stability outperforms the results derived from P–E loops, owing to the higher test frequency employed [2]. The increasing paraelectric phase fraction contributes to a higher discharge rate of MLCCs, leading to a reduction in $t_{0.9}$ as temperature increases. The temperature stability of P_D can be evaluated by the I_{max} of undamped discharge current curves ($P_D \propto I_{max}$) at various temperatures (Figs. 5(c) and 5(d)) [31,32]. According to the stable I_{max}, the P_D of MLCCs possesses excellent stability over the temperature range from 22 to 200 °C. The oscillation frequency (ω_0) of the undamped discharge current curves is determined by the resistance (R), capacitance (C), and inductance (L) of the circuit (Eq. (1)) [10]:

$$\omega_0 = \sqrt{1/(LC) - [R/(2L)]^2} \quad (1)$$

The capacitance of MLCCs decreases with increasing temperature, resulting in a rising ω_0 and a reducing oscillation period. The fatigue stability of the pulse properties for 1210-MLCCs was evaluated under undamped discharge conditions at 2000 V and various temperatures, as shown in Fig. S10 in the ESM. After 1000 cycles under 22 and 200 °C, the undamped discharge current curves show negligible changes. The I_{max} values remain stable at 65.8 A, demonstrating excellent fatigue stability at both room temperature and high temperature. To further evaluate the pulse properties, we fabricated 6878-size MLCCs with 100 active layers, as shown in Fig. 6. The capacitance of 6878-MLCCs is 300 nF. The I_{max} of the undamped discharge current curve under V_r and room temperature for 6878-MLCCs can achieve approximately 3600 A. To evaluate the breakdown resistance and reliability, the 6878-MLCCs were tested at a voltage withstand of 3600 V (1.2 times V_r) and underwent 50 cycles at V_r. No damage occurred in the 6878-MLCCs, indicating high breakdown strength and good reliability. A comparison of the capacitance-temperature behavior and pulsed discharge properties among 6878-MLCCs and common commercial MLCCs is presented in Table 2. Compared to commercial linear MLCCs, BT-based RFE MLCCs with the same structural design (6878-size, 100 layers, and floating inner electrode structure) achieve higher capacitance and release I_{max}, owing to the higher dielectric constant of RFE than that of

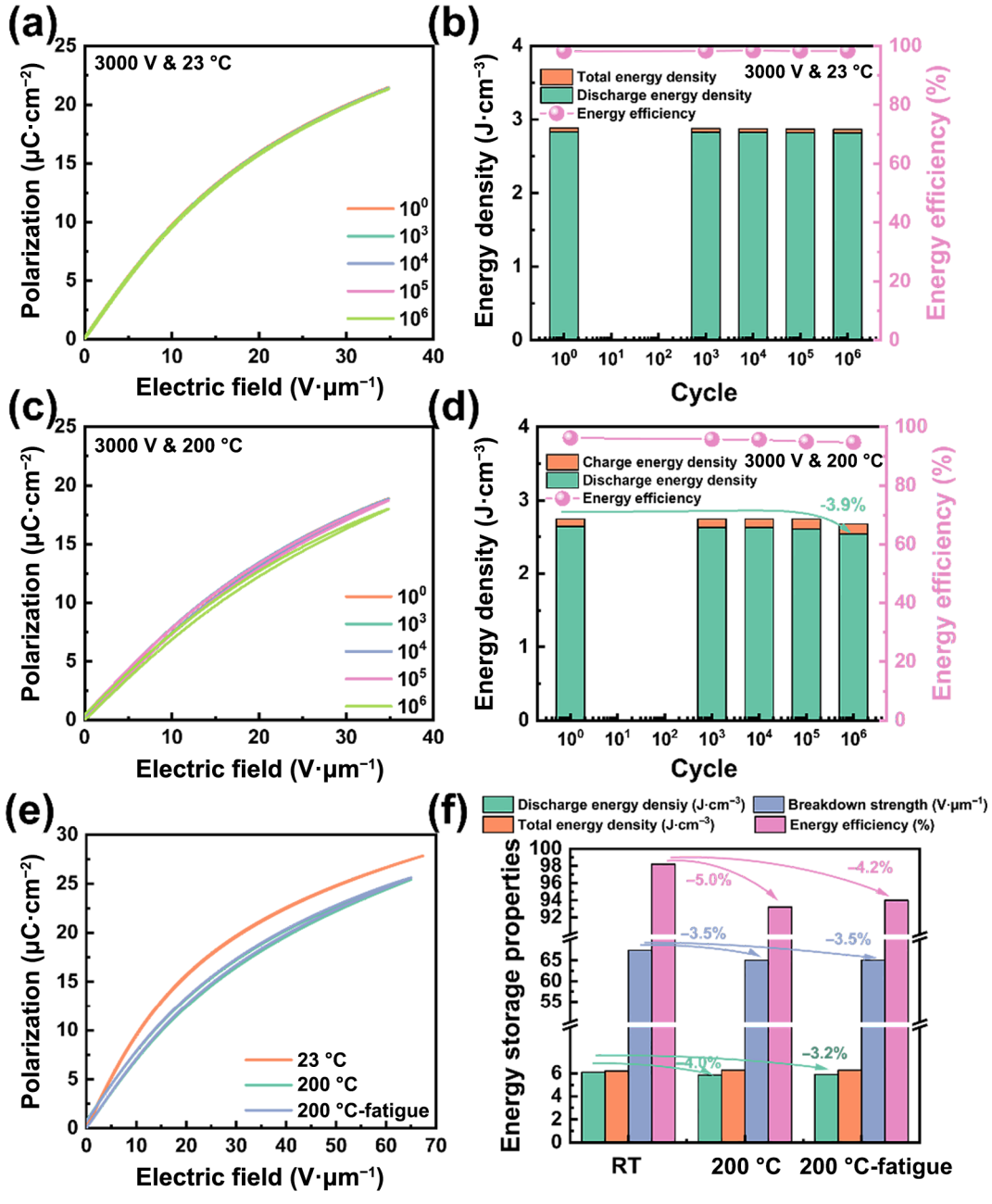

Fig. 4 Unipolar *P*–*E* loops of 1210-MLCCs under V_r as a function of cycling time and the corresponding energy-storage properties at (a, b) room temperature and (c, d) 200 °C. (e, f) Comparison of *P*–*E* loops with various 1210-MLCCs measured under different test conditions and the corresponding energy-storage properties.

Table 1 Comparison of the energy-storage properties measured with various 1210-MLCCs and different test conditions

Test condition	E_b (V·μm⁻¹)	W_d (J·cm⁻³)	W_t (J·cm⁻³)	η (%)
23 °C	67.4	6.09	6.20	98.2
200 °C	65.0	5.84	6.27	93.2
200 °C-fatigue	65.0	5.89	6.27	94.0

linear ceramics. Furthermore, the substitution of linear dielectrics with RFE reduces both the dielectric layers and the usage of noble metal inner electrodes without sacrificing energy density or discharge current, thus lowering the overall device cost. Pb-based AFE MLCCs are inherently limited in breakdown voltage by mechanical failure induced by the high strain of the field-induced phase transition (AFE phase to FE phase). However, AFE MLCCs must be operated above the phase transition electric field to deliver high capacitance and a large discharge current. Hence, the V_r of AFE MLCCs is usually set slightly above the phase transition threshold. In practice, the MLCCs generally operate below V_r. The narrow margin of AFE MLCCs makes it challenging to sustain high performance in complex and fluctuating operational environments. Free from obvious phase transition behavior under high electric fields, the RFE MLCCs enable low operating voltages while maintaining high capacitance and adequate discharge current. Moreover, BT-based RFE MLCCs show better capacitance-temperature behavior than Pb-based AFE MLCCs,

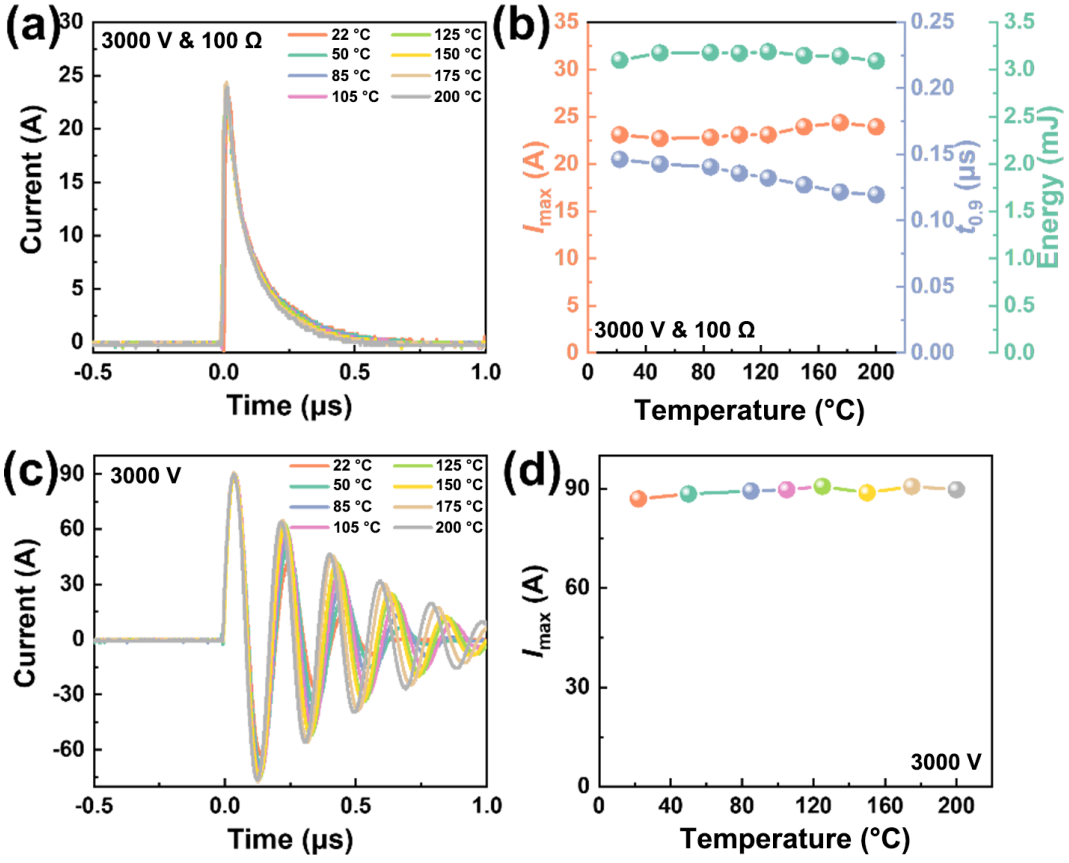

Fig. 5 (a) Temperature-dependent overdamped discharge current of MLCCs under V_r and (b) the corresponding properties. (c) Temperature-dependent undamped discharge current of MLCCs under V_r and (d) the corresponding pulse peak current values.

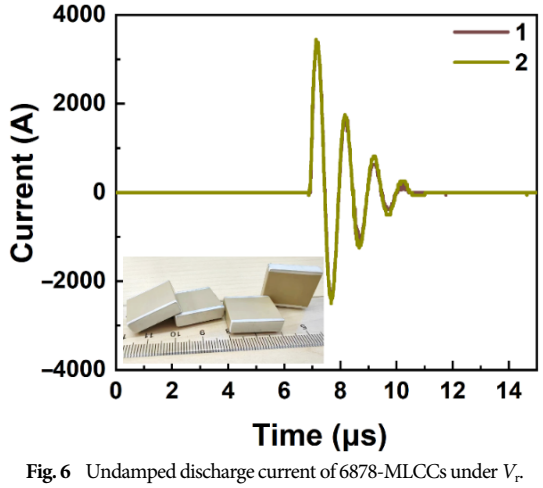

Fig. 6 Undamped discharge current of 6878-MLCCs under V_r.

making them more suitable for pulsed-power applications over a wide operating temperature range. Therefore, BT-based RFE MLCCs with superior pulse properties, temperature stability and fatigue stability are more promising for practical pulsed-power applications.

4 Conclusions

BT-based weakly coupled RFE MLCCs with floating inner electrode structures were fabricated for high-voltage applications. The temperature coefficient capacitance of RFE MLCCs satisfies the EIA X8R and X9S specifications, and a good W_d of 6.09 J cm^{-3} and an ultrahigh η of 98.2% are achieved at room temperature. The energy storage and pulse properties of MLCCs exhibit superior stability at a rated voltage of 3000 V. The W_d of MLCCs changes < 10% in the temperature range of 24–250 °C, while maintaining an η > 93%. The energy-storage properties also

Table 2 Comparisons of dielectric and pulse properties between our MLCCs and some commercial MLCCs

	Material system	Size and capacitance	TCC[1]	Pulse peak current@voltage
Commercial	Linear	4045-220 nF	−55 to 125 °C −2200±250 ppm °C^{-1}	1.6–2.0 kA@2.0 kV
	Linear	6878-220nF	−55–125 °C −2200±250 ppm °C^{-1}	2.6–3.0 kA@3.0 kV
	Pb-based AFE	3040-120 nF	−55–125 °C −10%–45%	1.9 kA@1.25 kV
This work	**BT-based RFE**	**6878-300 nF**	**X8R[2]/X9S[3]**	**3.6 kA@3.0 kV**

Note: [1]TCC–temperature coefficient of capacitance (TCC=(C_T/$C_{25\,°C}$)/$C_{25\,°C}$ × 100%, where C_T is the capacitance (C) at the temperature (T));
[2]X8R–TCC ≤ ±15% over temperature range from −55 to 150 °C;
[3]X9S–TCC ≤ ±22% over temperature range from −55 to 200 °C.

possess excellent fatigue stability and reliability, showing < 4% degradation after 10^6 cycles even at 200 °C. The overdamped and undamped pulsed discharge current curves exhibit negligible variation between 22 and 200 °C. Furthermore, the 6878-size MLCCs with a capacitance of 300 nF release a peak current of 3600 A. The combination of high power and superior stability makes the RFE MLCCs a promising candidate for advanced energy storage and pulsed power systems, showing strong potential for further development.

Acknowledgements

This work was supported by the National Natural Science Foundation of China (Nos. 52472130, 52502139, and 52372101), the Program of High-Performance Dielectric/Conductive Materials (No. CEIEC-2024-ZM02-0052), Tsinghua University State Key Laboratory of New Ceramic Materials Project (No. 2025QHTC-ZZKYB002), and the Fundamental Research Funds for the Beijing University of Posts and Telecommunications (No. 2025JCTP05).

Author contributions

Peiyao Zhao: Writing – original draft, data curation, validation, methodology, funding acquisition; Ying Jiang: Data curation, validation; Hongxian Wang: Methodology, data curation; Limin Guo: Writing – review & editing, formal analysis, funding acquisition; Xiaohui Wang: Supervision, funding acquisition.

Availability of data and materials

The data that support the findings of this study are available from the corresponding author upon reasonable request.

Competing interests

The authors have no competing interests to declare that are relevant to the content of this article. The author Xiaohui Wang is the Editorial Committee member of this journal.

Electronic Supplementary Material

Supplementary material is available in the online version of this article at https://doi.org/10.26599/JAC.2026.9221264.

References

[1] Wang G, Lu ZL, Li Y, *et al.* Electroceramics for high-energy density capacitors: Current status and future perspectives. *Chem Rev* 2021, **121**: 6124–6172.
[2] Yang LT, Kong X, Li F, *et al.* Perovskite lead-free dielectrics for energy storage applications. *Prog Mater Sci* 2019, **102**: 72–108.
[3] Yan F, Qian J, Wang SM, *et al.* Progress and outlook on lead-free ceramics for energy storage applications. *Nano Energy* 2024, **123**: 109394.
[4] Yang BB, Liu YQ, Jiang RJ, *et al.* Enhanced energy storage in antiferroelectrics via antipolar frustration. *Nature* 2025, **637**: 1104–1110.
[5] Zubairi H, Lu ZL, Zhu YB, *et al.* Current development, optimisation strategies and future perspectives for lead-free dielectric ceramics in high field and high energy density capacitors. *Chem Soc Rev* 2024, **53**: 10761–10790.
[6] Dai SW, Li MY, Wu XW, *et al.* Combinatorial optimization of perovskite-based ferroelectric ceramics for energy storage applications. *J Adv Ceram* 2024, **13**: 877–910.
[7] Zhang M, Lan S, Yang BB, *et al.* Ultrahigh energy storage in high-entropy ceramic capacitors with polymorphic relaxor phase. *Science* 2024, **384**: 185–189.
[8] Zhao PY, Cai ZM, Wu LW, *et al.* Perspectives and challenges for lead-free energy-storage multilayer ceramic capacitors. *J Adv Ceram* 2021, **10**: 1153–1193.
[9] Hong K, Lee TH, Suh JM, *et al.* Perspectives and challenges in multilayer ceramic capacitors for next generation electronics. *J Mater Chem C* 2019, **7**: 9782–9802.
[10] Xu CH, Liu Z, Chen XF, *et al.* High charge-discharge performance of $Pb_{0.98}La_{0.02}(Zr_{0.35}Sn_{0.55}Ti_{0.10})_{0.995}O_3$ antiferroelectric ceramics. *J Appl Phys* 2016, **120**: 074107.
[11] Milliken AD, Bell AJ, Scott JF. Dependence of breakdown field on dielectric (interelectrode) thickness in base-metal electroded multilayer capacitors. *Appl Phys Lett* 2007, **90**: 112910.
[12] Qi H, Xie AW, Zuo RZ. Local structure engineered lead-free ferroic dielectrics for superior energy-storage capacitors: A review. *Energy Storage Mater* 2022, **45**: 541–567.
[13] Pan H, Li F, Liu Y, *et al.* Ultrahigh–energy density lead-free dielectric films via polymorphic nanodomain design. *Science* 2019, **365**: 578–582.
[14] Pan H, Lan S, Xu SQ, *et al.* Ultrahigh energy storage in superparaelectric relaxor ferroelectrics. *Science* 2021, **374**: 100–104.
[15] Zhao WC, Liu ZB, Xu DM, *et al.* Advanced stability and energy storage capacity in hierarchically engineered $Bi_{0.5}Na_{0.5}TiO_3$-based multilayer capacitors. *Nat Commun* 2025, **16**: 6549.
[16] Zhou ZX, Bai WF, Liu N, *et al.* Ultrahigh capacitive energy storage of $BiFeO_3$-based ceramics through multi-oriented nanodomain construction. *Nat Commun* 2025, **16**: 2075.
[17] Li D, Xu DM, Zhao WC, *et al.* A high-temperature performing and near-zero energy loss lead-free ceramic capacitor. *Energy Environ Sci* 2023, **16**: 4511–4521.
[18] Yang Y, Xu K, Yang B, *et al.* Giant energy storage density with ultrahigh efficiency in multilayer ceramic capacitors *via* interlaminar strain engineering. *Nat Commun* 2025, **16**: 1300.
[19] Xie AW, Li ZH, Wu X, *et al.* Superior capacitive energy storage of $NaNbO_3$-based MLCCs enabled by heterogeneous short-range ferroic orders. *Adv Funct Mater* 2026, **36**: 16297.
[20] Fu J, Xie AW, Zuo RZ, *et al.* A highly polarizable concentrated dipole glass for ultrahigh energy storage. *Nat Commun* 2024, **15**: 7338.
[21] Lv ZQ, Lu T, Liu Z, *et al.* $NaNbO_3$-based multilayer ceramic capacitors with ultrahigh energy storage performance. *Adv Energy Mater* 2024, **14**: 2304291.
[22] Qi JL, Zhang MH, Chen YY, *et al.* High-entropy assisted $BaTiO_3$-based ceramic capacitors for energy storage. *Cell Rep Phys Sci* 2022, **3**: 101110.
[23] Zhao PY, Wang HX, Wu LW, *et al.* High-performance relaxor ferroelectric materials for energy storage applications. *Adv Energy Mater* 2019, **9**: 1803048.
[24] Wang Y, Chan YC, Gui ZL, *et al.* Application of Weibull distribution analysis to the dielectric failure of multilayer ceramic capacitors. *Mater Sci Eng B* 1997, **47**: 197–203.
[25] Yuan QB, Chen M, Zhan SL, *et al.* Ceramic-based dielectrics for electrostatic energy storage applications: Fundamental aspects, recent progress, and remaining challenges. *Chem Eng J* 2022, **446**: 136315.
[26] Yang ZT, Du HL, Jin L, *et al.* Realizing high comprehensive energy storage performance in lead-free bulk ceramics via designing an unmatched temperature range. *J Mater Chem A* 2019, **7**: 27256–27266.
[27] Li JL, Li F, Xu Z, *et al.* Multilayer lead-free ceramic capacitors with ultrahigh energy density and efficiency. *Adv Mater* 2018, **30**: 1802155.
[28] Wang XZ, Song XJ, Fan YB, *et al.* Lead-free high permittivity quasi-linear dielectrics for giant energy storage multilayer ceramic capacitors with broad temperature stability. *Adv Energy Mater* 2024, **14**: 2400821.
[29] Sun ZX, Diwu L, Gao RY, *et al.* Machine learning-driven ultra-high energy storage performance in ferro-superparaelectric capacitors. *Adv Funct Mater* 2026, **36**: 16412.
[30] Xie AW, Fu J, Zuo RZ, *et al.* Supercritical relaxor nanograined ferroelectrics for ultrahigh-energy-storage capacitors. *Adv Mater* 2022, **34**: 2204356.
[31] Huan Y, Gui DY, Li CX, *et al.* Simultaneously enhanced energy storage performance and luminance resistance in $(K_{0.5}Na_{0.5})NbO_3$-based ceramics *via* synergistic optimization strategy. *J Adv Ceram* 2024, **13**: 34–43.
[32] Xu LY, Ouyang J, Cheng ZX, *et al.* A review on the dielectric ceramics for high energy-storage application. *Adv Ceram* 2025, **46**: 195–246. (in Chinese)